IEEE Access
Multidisciplinary | Rapid Review | Open Access Journal

Received October 10, 2021, accepted October 26, 2021, date of publication October 28, 2021, date of current version November 8, 2021.

Digital Object Identifier 10.1109/ACCESS.2021.3124162

A Blind Demodulation Algorithm for Underwater Acoustic MPSK Signal

LULU WU, BIN WANG, YAN HUANG, HAIWANG WANG, AND QIANG TANG
PLA Strategic Support Force Information Engineering University, Zhengzhou 450001, China
Corresponding author: Bin Wang (oceansgroup2020@163.com)

ABSTRACT Multiple phase-shift keying (MPSK) is a common carrier modulation in underwater acoustic (UWA) communication. This paper proposes a robust blind demodulation algorithm to improve the performance and practicability of blind demodulation of MPSK signals under impulsive noise and UWA sparse multipath channels. The proposed algorithm adopts a $T/2$-spaced blind equalizer based on quasi-affine projection, so it has strong adaptability to sparse UWA multipath channels. First, the received signal is preprocessed to suppress the impulsive interference, and the parameters are estimated. Then, timing synchronization is performed point by point based on sliding discrete Fourier transform (SDFT) to avoid equalizer performance degradation or even lock-loss caused by large clock frequency deviation and long-time error accumulation. Based on this, the over-sampling signal with two fixed sampling points per symbol is obtained. Meanwhile, following the idea of memory improved proportionate affine projection algorithm and normalized factor, the cost function of the blind equalizer is constructed by using the l_0 norm penalty on the tap coefficients. In this way, the updating formula of the tap coefficients is derived, and the blind equalization is then conducted on the signal after timing synchronization to eliminate or weaken the channel influence. Finally, the residual frequency offset and phase offset of the carrier are removed through the M-power transform and the second-order decision feedback digital phase-locked loop. Simulation experiments and practical signal demodulation results indicate that the proposed algorithm achieves higher BER performance and modulation parameter robustness for impulsive noise and UWA multipath channel.

INDEX TERMS Impulsive noise, underwater acoustic communication, MPSK, blind demodulation, fractionally spaced, sliding discrete Fourier transform.

I. INTRODUCTION

Multiple phase-shift keying (MPSK) signal has the advantages of high band efficiency and strong anti-noise ability, so it is widely used in underwater acoustic (UWA) communication. In non-cooperative reception applications such as underwater information monitoring and UWA countermeasure, UWA signals often need to be processed without or with little prior information. The blind demodulation of UWA MPSK signals is important for such applications.

Multipath effect is one of the major reasons of signal distortion in UWA communication, and causes time delay spread and frequency selective fading. The distortion is usually represented as inter-symbol interference (ISI). To reduce or eliminate ISI, the equalization technique is usually used in blind demodulation. Compared with the traditional non-blind equalization, blind equalization can improve the band efficiency of limited bandwidth and does not need a training sequence. Therefore, blind equalization is more suitable for the application scenarios where prior information cannot be obtained. The UWA channel is different from radio communication channel and has a long delay spread and typical sparse characteristics [1]. Also, the energy of the channel impulse response is concentrated on a few taps far apart, and most taps are very small or even equal to zero. Besides, the ambient noise is often impulsive due to the influence of man and marine life. In recent years, some new algorithms for blind equalization of UWA MPSK signals have been proposed [2]–[4]. For example, a variable observation window length (VOWL) blind equalization algorithm based on the multi-modulus algorithm (MMA) was proposed in [3]. The advantage of this algorithm is that the order of the blind equalizer can be dynamically adjusted to the best according to the characteristics of UWA channel. A variable step-size dual-mode blind equalization algorithm was proposed in [4]. The step size is controlled by introducing inverse

The associate editor coordinating the review of this manuscript and approving it for publication was Prakasam Periasamy.

hyperbolic sine function, and the algorithm has good anti-noise performance. However, both algorithms do not consider the sparse characteristics of the UWA channel, and their performance decreases seriously when the channel has a long delay and deep-fading characteristics. For the sparsity of the UWA channel, integrating the l_0 norm of the equalizer tap coefficient vector into the cost function as a penalty term is a superior approach. The redundant coefficients (the coefficients close to zero after convergence) can be forced to update adaptively to zero. These algorithms are less affected by humans, and the difficulty lies in the selection of norms. Besides, a blind equalization algorithm based on multi-modulus decision feedback equalizer and l_0 norm constraint (l_0-MMBDFE) was proposed in [2]. The advantage of this algorithm is that it can adjust the value of zero attractor according to the power of the measured noise. In addition, a variable step-size blind equalization algorithm based on the l_0 norm constraint was proposed in [5]. The algorithm adaptively updates the step size by using the normalized proportionate factor. Although these algorithms can better compensate the UWA channels, they still have the problems of slow convergence and large residual ISI. It is acknowledged that the blind equalization based on affine projection algorithm (APA) can achieve a good tradeoff between computational complexity and convergence speed [6]–[8]. Currently, there are few practical algorithms for blind demodulation of UWA MPSK signals in the open literature, and most of the existing studies only discuss the blind equalization links of the blind demodulation. Although some algorithms take the bit error rate (BER) performance of the demodulation into consideration, they do not consider the influence of symbol time offset, carrier frequency offset, and clock frequency deviation. Thus, they cannot be directly applied to the blind demodulation of practical MPSK signals in a complex environment. Overall, there is a lack of a complete and practical blind demodulation algorithm for MPSK signals with impulsive noise.

To solve the above problems, a blind demodulation algorithm for MPSK signals with UWA multipath channel and impulsive noise is proposed in this paper. First, the algorithm preprocesses the received signal, such as adaptive clipping, parameters estimation. Then, a sampling point-by-point timing synchronization algorithm based on sliding discrete Fourier transform (SDFT) is proposed to compensate for the sampling phase deviation caused by clock frequency deviation and UWA channel. The SDFT-based synchronization can make the algorithms in [2]–[5] more applicable to the scenario with a large clock frequency deviation and a complex channel. Based on this, the signal with two fixed sampling points per symbol is obtained as the input of the $T/2$-spaced blind equalizer. To increase the convergence speed and decrease the residual error of the equalizer, a fractionally spaced blind equalization algorithm based on quasi-affine projection algorithm (QAPA) with l_0 norm constraint is proposed. The algorithm has strong adaptability and compensation capacity for the UWA channel with sparse and deep-fading characteristics. Also, it can keep the residual error low while converging fast. Finally, carrier synchronization is realized based on M-power transform and digital phase-locked loop (DPLL), and then the original information is recovered. Simulation and practical signals blind demodulation results indicate that, compared with the existing algorithms, the proposed blind demodulation algorithm has better BER performance and ability against multi-path interference of the UWA channels.

This paper proposes a new approach for the blind demodulation of UWA MPSK signals. The contributions of this work are summarized as follows:

- The performance of the existing blind equalization algorithm deteriorates in the sparse deep-fading UWA channel. In comparison, the proposed algorithm combines the advantages of proportionate-type APA, fractionally spaced equalizer (FSE), and l_0 norm, so it outperforms other algorithms.
- Most of the existing algorithms do not consider the influence of clock frequency deviation on the signal, so their practicability is poor. However, this paper derives a sampling point-by-point timing recovery algorithm based on SDFT. The algorithm can avoid equalizer performance degradation or even lock-loss, and it is more robust in UWA multipath channels.
- This paper presents a complete blind demodulation scheme from frequency band signal to bitstream, which can be directly applied to engineering practice. In comparison, the existing methods are based on the baseband signal model, and they are far from practical applications.

The remainder of this paper is organized as follows. The signal model is introduced in Section II. Then, the proposed algorithm and the details are presented in Section III. The simulation results and field experiments are given in Section IV and V, respectively. Finally, the paper is concluded in Section VI.

II. SIGNAL MODEL

In this paper, it is assumed that there is no relative motion between the receiver and the sender under good conditions. Under this assumption, only the influence of multipath transmission and ambient noise on communication is considered, and the received signal can be modeled as:

$$y(n) = s(n) \otimes h'(n) + u(n) \tag{1}$$

where n is the sampling time; $y(n)$ is the received signal; $h'(n)$ is the impulse response of the UWA channel; $u(n)$ is the ambient noise, and $\otimes$ represents the convolution operation. $s(n)$ is the MPSK modulated signal to be transmitted, and it can be expressed as

$$s(n) = Ae^{j\theta} e^{j2\pi f_c n T_s} \sum_i b_i g(n - iT - \tau) \tag{2}$$

where A, T, $T_s = 1/f_s$, f_c, θ, and τ respectively denote the signal amplitude, symbol period, sampling period,

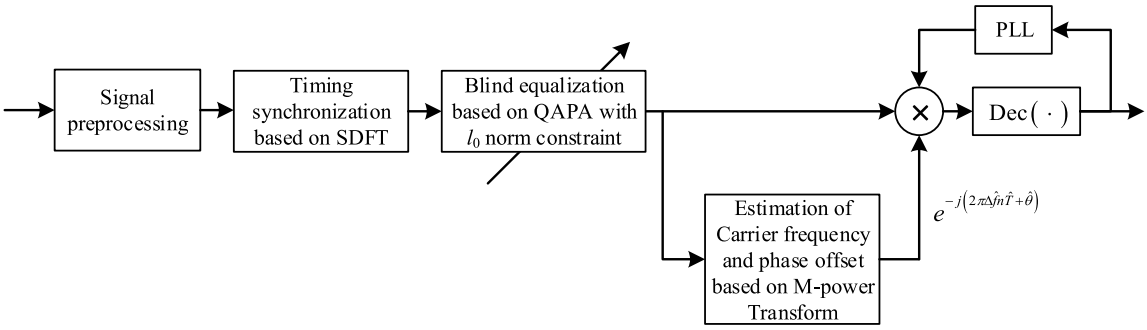

FIGURE 1. The block diagram of the blind demodulation algorithm for the UWA MPSK signal.

carrier frequency, carrier phase, and transmission delay. The baseband symbol sequence $\{b_i\}$ is complex-valued independent and identically distributed (i.i.d.), where $b_i \in \{\tilde{b}_m | \tilde{b}_m = e^{j2\pi(m-1)/M}, m = 1, \cdots, M\}$ is the i-th symbol and M is the modulation order of the MPSK signal.

To fully reflect the characteristics of actual marine ambient noise, $u(n)$ is usually modeled as alpha-stable distribution noise. The characteristic exponent of the alpha-stable distribution noise indicates the intensity of the impulsive noise. The smaller the characteristic exponent, the stronger the impulsive ambient noise. When the characteristic exponent takes the maximum value of 2, it indicates that the ambient noise has a Gaussian distribution. This model can substantially reflect the complexity of actual marine ambient noise, and it is a practical modeling method for a wide range of applications. Specifically, the characteristic function of alpha-stable distribution noise is [9]:

$$\phi(u) = \exp\left(jbu - \varpi |u|^{\alpha}\left[1 + j\phi \mathrm{sgn}(u)\omega(u, \alpha)\right]\right) \quad (3)$$

where, $\alpha \in (0, 2]$ is the characteristic exponent, and a smaller α corresponds to more significant impulsive characteristics. In fact, the characteristic exponent α of most ambient noise in the ocean is in the range of 1.6 to 2.0 [10], [11]. The location parameter b determines the center axis of the distribution function, and the dispersion coefficient ϖ is used to measure the degree to which the distribution deviates from its mean. The skew parameter ϕ describes the degree of symmetry of the distribution. When $\phi = 0$, the distribution is symmetric about b and is called symmetric alpha-stable distribution. When $b = 0$ and $\varpi = 1$, the distribution belongs to standard alpha-stable distribution. For simplicity, the standard alpha-stable distribution is considered in this paper.

Since there are no limited second-order or higher-order moments in the alpha-stable distribution when $\alpha < 2$, the mixed signal-to-noise ratio (MSNR) is usually adopted to measure the power relationship between the signal and noise. MSNR can be expressed as:

$$MSNR = 10\lg\left(\sigma_s^2/\varpi\right)(\mathrm{dB}) \quad (4)$$

where σ_s^2 is the variance of signal $s(n)$.

III. BLIND DEMODULATION ALGORITHM FOR UNDERWATER ACOUSTIC MPSK SIGNAL

Ocean ambient noise and multipath effect are the main factors affecting the demodulation performance of UWA MPSK signals. In this paper, a blind demodulation algorithm for UWA MPSK signal is proposed by suppressing the ambient noise and improving the performance of timing recovery and blind equalization. The schematic diagram of the algorithm is shown in Fig. 1.

First, the received signal is preprocessed, including adaptive impulsive noise suppression, the estimation of carrier frequency and symbol rate, and down-conversion. Second, the SDFT-based timing synchronization is conducted to obtain the basepoint and the fractional delay of each half-symbol period, and the signal with two fixed sampling points per symbol could be obtained. Then, based on the structure of FSE, the cost function is constructed by imposing an l_0 norm penalty on the tap coefficients of the equalizer. Also, the updating formula of the tap coefficients is derived following the idea of memory improved proportionate APA (MIPAPA) and normalized factor. Subsequently, the twice-oversampled signal is input into the blind equalizer to compensate for the channel. The output of the equalizer is the baseband symbols with a frequency offset and a circle-shaped constellation. Finally, the frequency and phase offset are roughly estimated and compensated by using the M-power transform. Then, the carrier phase is tracked by the second-order decision feedback DPLL to remove the tiny frequency and phase offset. In this way, the original information can be recovered after the hard decision of the obtained constellation symbols. In Fig. 1, Dec $(\cdot)$ denotes the hard decision operation.

A. PREPROCESSING OF RECEIVED SIGNAL

There are no limited second-order and higher-order statistics in alpha-stable distribution when $\alpha < 2$. Thus, the fractional low-order processing and impulsive noise suppression followed by second-order or higher-order statistical processing is usually used. The former depends on the accurate estimation of noise characteristic exponent of alpha-stable distribution, and the calculation process is complicated. The latter often uses different nonlinear transforms to suppress the impulsive noise according to specific demands.

The impulsive intensity of the noise is reduced, and then the noise is processed as Gaussian noise.

By contrast, the latter has more practical value in engineering applications and is adopted by this paper to suppress impulsive noise through an adaptive threshold.

The key of suppressing impulsive noise by using nonlinear transformation is to construct a nonlinear transform function. In this paper, the median-based adaptive threshold suppression algorithm proposed in [12] is used to suppress impulsive noise. The algorithm sets the threshold adaptively. It takes the signal sampling values larger than the threshold as impulsive interference. Then, the values are multiplied by the adaptive attenuation factor to suppress strong impulsive interference.

The adaptive threshold can be expressed as:

$$th = (1 + 2\tau_0) \cdot \text{median}(\boldsymbol{y}_{abs}) \tag{5}$$

where τ_0 is a constant and median$(\cdot)$ represents the median function. Based on the threshold, strong impulsive interference suppression is performed according to (6).

$$y'(n) = \begin{cases} y(n)\left(\dfrac{th}{|y(n)|}\right)^2 & |y(n)| \geq th \\ y(n) & |y(n)| < th \end{cases} \tag{6}$$

where $y'(n)$ is the signal after impulsive noise suppression. Then, the carrier frequency is roughly estimated by the frequency mediacy algorithm based on the welch spectrum [13], and the down-conversion is conducted. The signal after down-conversion has periodicity because it contains the periodic component of the symbol. Also, the amplitude spectrum of the signal has a discrete spectral line at the symbol rate, from which the symbol rate can be estimated. Besides, a matched filter can be designed to improve the SNR at the sampling time. The roll-off factor is usually set to 0.35.

B. TIMING SYNCHRONIZATION BASED ON SDFT

The traditional forward timing synchronization algorithms adjusting sampling time are derived based on maximum likelihood under the condition of Gaussian white noise. They can work in fading channels, but the estimation accuracy is greatly affected. In radio communication, joint equalization and timing recovery are conducted based on FSE in [14]. Under a long-time accumulation of the clock frequency deviation and timing error, the coefficients of FSE will shift. These algorithms usually adjust the coefficients by shifting the taps based on the relationship between the center of mass (COM) and central position (CP) of the equalizer. For a large clock frequency deviation, the channel changes rapidly, making it crucial to put forward blind equalization algorithms with a fast-tracking capacity. Besides, due to the sparsity of the UWA channel, the distribution of the blind equalizer taps is also sparse, so the expected value of COM is not always in the center of the taps. Therefore, the above algorithms cannot be directly applied to the blind demodulation of MPSK signals in the complex condition with UWA multipath channel and impulsive noise.

To overcome the influence of clock frequency deviation and error accumulation stably and reliably, an effective and low-complexity algorithm is proposed in this paper. For signals $r(n)$ with carrier frequency offset after matched filtering, the timing phase estimation is conducted by using the O&M algorithm [15]. This algorithm is insensitive to carrier frequency offset, and its expression is shown as follows:

$$\hat{\varepsilon}_n = -\frac{1}{2\pi} \arg\left[\sum_{n=mL_0p}^{(m+1)L_0p-1} |r(n)|^2 e^{-j2\pi n/r}\right] \tag{7}$$

where $\hat{\varepsilon}_n \in [0, 1)$ is the estimated value of the normalized timing phase; L_0 is the number of symbols; p is the oversampling factor that needs to satisfy $p > 2$. In practice, $p = 4$ is usually taken. However, under the influence of the multipath channel, the timing phase estimation obtained by this algorithm is biased. Considering this problem, this paper uses sampling point-by-point timing phase estimation to reduce the influence of multipath channels. Meanwhile, SDFT iteration is introduced to greatly reduce the computational complexity. Based on this, each sampling point only needs four real multiplications and four real additions. The iterative formula is shown as follows:

$$Y_n = e^{j2\pi k_B/(L_0p)}\left[Y_{n-1} + r_a(n) - r_a(n - L_0p)\right] \tag{8}$$

where, $r_a(n) = |r(n)|^2$, $k_B = L_0p \cdot \hat{R}_B/f_s$, and $\hat{R}_B$ is the estimation of symbol rate. $Y_0 = Y(k_B)$, where $Y(k)$ represents the FFT sequence of the first L_0p points of $r_a(n)$. Therefore, the timing phase of the n-th sampling point can be estimated as follows:

$$\hat{\varepsilon}_n = -\frac{1}{2\pi} \arg(Y_n) \tag{9}$$

The basepoint m_i and fractional delay μ_i of each half-symbol period can be obtained following the timing estimator interpolation control algorithm [16]. Then both parameters are adjusted by timing phase estimation error in each symbol period. The iterative formulas are as follows

$$m_{i+1} = m_i + \left\lfloor \mu_i + \frac{\hat{T}}{T_s}\left[0.5 + l \cdot \text{SAW}\left(\hat{\varepsilon}_n - \hat{\varepsilon}_{n-1}\right)\right] \right\rfloor \tag{10}$$

$$\mu_{i+1} = \left\{ \mu_i + \frac{\hat{T}}{T_s}\left[0.5 + l \cdot \text{SAW}\left(\hat{\varepsilon}_n - \hat{\varepsilon}_{n-1}\right)\right] \right\}_{\text{mod } 1} \tag{11}$$

where $\lfloor \cdot \rfloor$ indicates rounding-down operation; $\hat{T} = 1/\hat{R}_B$ is the estimated value of the symbol period, and the basepoint m_i is the smallest integer n that satisfies $i\hat{T}/2 \geq nT_s$; SAW $(\cdot)$ denotes the sawtooth wave function with a period of 1; $\mu_i = i\hat{T}/T_s - m_i$ is the fractional delay, and $\mu_i \in [0, 1)$. l is used to control the time of adjusting timing error, and it is expressed as:

$$l = \begin{cases} 1, & \text{mod}(n, p) = 0 \\ 0, & else \end{cases} \tag{12}$$

The signal with two fixed sampling points per symbol can be obtained by interpolation processing [17] based on the

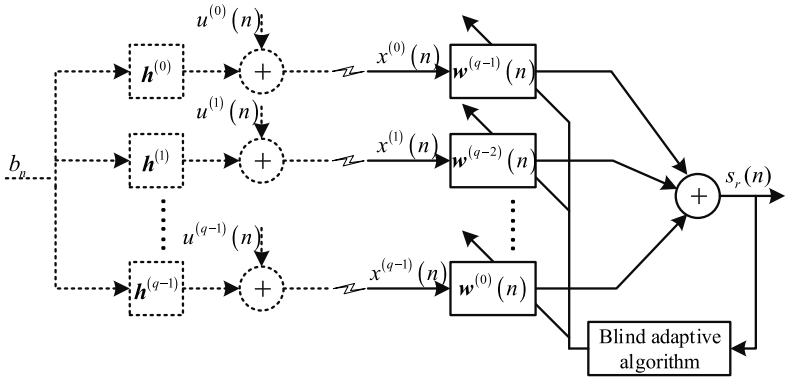

FIGURE 2. The system model of the blind FSE.

basepoint and fractional delay of each half-symbol period. Then, the signal is input to the QAPA-based $T/2$-spaced equalizer with l_0 norm constraint for blind equalization. Finally, the baseband signal with frequency and phase offset can be obtained. In particular, for a large oversampling factor, there is no need for interpolation, and the sampling point closest to the basepoint is selected.

C. FRACTIONALLY SPACED BLIND EQUALIZATION BASD ON QAPA WITH L_0 NORM CONSTRAINT

FSE can effectively avoid the spectral aliasing problem caused by symbol rate sampling and compensate the channel with spectral nulls near the unit circle. The input of FSE is the signal oversampled at least as fast as the Nyquist rate. Also, FSE is insensitive to timing error and can achieve timing recovery and channel equalization at the same time [18], so the fractionally spaced blind equalization structure is adopted in this paper.

The multichannel model of the T/q-spaced equalizer based on equivalent baseband is shown in Fig. 2. $\boldsymbol{h}^{(i)} \triangleq \left[h_0^{(i)}, h_1^{(i)}, \cdots, h_{M_c-1}^{(i)}\right]^T$ is the i-th joint sub-channel impulse response based on T-spaced (or baud rate) $i = 0, 1, \cdots, q-1$; $\boldsymbol{x}(n) = \left[x^{(0)}(n), x^{(1)}(n), \cdots, x^{(q-1)}(n)\right]^T$ denotes the received signal vector at instant n after timing synchronization. Through the preprocessing of the suppression, the influence of strong impulsive interference is greatly reduced, and the noise can be treated as Gaussian noise. We define the vector $\boldsymbol{w}_j(n) \triangleq \left[w_j^{(q-1)}(n),\ w_j^{(q-2)}(n), \cdots, w_j^{(0)}(n)\right]^T$ whose element $w_j^{(i)}(n)$ represents the j-th tap coefficient of the i-th sub-equalizer, $j = 0, 1, \cdots, N-1$ and $N \geq M_c$. Then the output of the blind equalizer can be represented as

$$s_r(n) = \boldsymbol{w}^{\mathrm{H}}(n)\,\bar{\boldsymbol{x}}(n) \tag{13}$$

where $\boldsymbol{w}(n) = \left[\boldsymbol{w}_0^T(n), \boldsymbol{w}_1^T(n), \cdots, \boldsymbol{w}_{N-1}^T(n)\right]^{\mathrm{T}}$ is the tap coefficient vector of the FSE, whose order is qN; $\bar{\boldsymbol{x}}(n) = \left[\boldsymbol{x}^T(n), \boldsymbol{x}^T(n-1), \cdots, \boldsymbol{x}^T(n-N+1)\right]^T$ is the total FSE input vector; $(\cdot)^T$ and $(\cdot)^H$ represent the transpose and conjugate transpose operations, respectively. In this paper, we take $q = 2$.

1) COST FUNCTION OF BLIND EQUALIZER

APA is an extension of normalized least mean square (LMS) algorithm. The key thought of APA is to keep the tap coefficient vector at the next instant $\boldsymbol{w}(n+1)$ as close as possible to the current one while forcing the posterior error to be zero. Following the sparse adaptive filter theory, by imposing the sparsity constraint on the equalizer coefficients, then the optimization problem can be expressed as:

$$\begin{aligned} &\min \|\boldsymbol{w}(n+1) - \boldsymbol{w}(n)\|^2 + \gamma \|\boldsymbol{w}(n+1)\|_0 \\ &\text{subject to } \boldsymbol{d}(n) - \boldsymbol{X}^{\mathrm{T}}(n)\,\boldsymbol{w}^*(n+1) = \boldsymbol{0} \end{aligned} \tag{14}$$

where $\boldsymbol{X}(n) = [\bar{\boldsymbol{x}}(n), \bar{\boldsymbol{x}}(n-1), \cdots, \bar{\boldsymbol{x}}(n-L+1)] \in \mathbb{R}^{qN\times L}$ is the block input matrix; L is the projection order; $\gamma > 0$ is the weight factor to the l_0 norm penalty; $\boldsymbol{d}(n)$ denotes the desired vector and $\|\boldsymbol{a}\|^2 \triangleq \boldsymbol{a}^H\boldsymbol{a}$. By adopting the idea of [8], the cost function of the proposed algorithm can be written as

$$\begin{aligned} J(n) = &\left(\frac{1}{\mu} - 1\right)\|\boldsymbol{w}(n+1) - \boldsymbol{w}(n)\|^2 \\ &+ \left\|\boldsymbol{d}(n) - \boldsymbol{X}^T(n)\,\boldsymbol{w}^*(n+1)\right\|^2_{A(n)} \\ &+ \gamma\|\boldsymbol{w}(n+1)\|_0 \end{aligned} \tag{15}$$

where $\|\boldsymbol{a}\|^2_{\boldsymbol{A}(n)} = \boldsymbol{a}^H\boldsymbol{A}(n)\,\boldsymbol{a}, \boldsymbol{A}(n) \triangleq \left[\boldsymbol{X}^H(n)\boldsymbol{X}(n) + \delta\boldsymbol{I}_L\right]^{-1}$; $\boldsymbol{s}_r(n) \triangleq \boldsymbol{X}^T(n)\,\boldsymbol{w}^*(n)$ is the output vector of the blind FSE, and $\boldsymbol{e}(n) = \boldsymbol{d}(n) - \boldsymbol{s}_r(n)$ is the prior error vector. Based on the constant modulus (CM) criterion, $\|\boldsymbol{e}(n)\|^2$ is minimized when $\boldsymbol{d}(n)$ takes the same direction as $\boldsymbol{X}^H(n)\,\boldsymbol{w}(n)$. Thus, $\boldsymbol{d}(n) = \mathrm{sgn}\left[\boldsymbol{X}^H(n)\,\boldsymbol{w}(n)\right]$, where $\mathrm{sgn}(a) = a/|a|$, $a \in \mathbb{C}$ and $\mathrm{sgn}(0) = 1$. $\boldsymbol{I}_L$, $\delta > 0$, and μ denote identity matrix, regularization factor, and step size, respectively.

2) ITERATIVE UPDATE OF TAP COEFFICIENTS OF BLIND EQUALIZER

By setting $\nabla_{\boldsymbol{w}^*(n+1)}J(n) = 0$, the coefficient updating formula can be obtained as follows

$$\begin{aligned} \boldsymbol{w}(n+1) = &\boldsymbol{w}(n) + \mu\boldsymbol{X}(n)\boldsymbol{A}(n)\boldsymbol{e}^*(n) \\ &- \boldsymbol{\kappa}\left[\boldsymbol{I}_{qN} - \mu\boldsymbol{X}(n)\boldsymbol{A}(n)\boldsymbol{X}^H(n)\right]\nabla_{\boldsymbol{w}^*} \\ &\times \|\boldsymbol{w}(n+1)\|_0 \end{aligned} \tag{16}$$

where $\boldsymbol{\kappa} = \mu\gamma/(1-\mu)$, and $\boldsymbol{I}_{qN}$ is an identity matrix. When $\mu = 1, \boldsymbol{I}_{qN} - \mu\boldsymbol{X}(n)\boldsymbol{A}(n)\boldsymbol{X}^H(n)$ is the orthogonal projector, and the third term on the right of (16) represents the projection of $\nabla_{\boldsymbol{w}^*}\|\boldsymbol{w}(n+1)\|_0$ onto the orthogonal complement within the range of $\boldsymbol{X}(n)$ (i.e., the null space of $\boldsymbol{X}^H(n)$). Left-multiplying (16) by $\boldsymbol{X}^H(n)$, we have $\boldsymbol{X}^H(n)\boldsymbol{w}(n+1) = \boldsymbol{d}(n)$, that is, the posterior error is zero as expected. When $0 < \mu < 1$, the posterior error is no longer equal to zero, and a compromise between the convergence speed and the misadjustment is achieved by adjusting μ. In effect, if there is measurement noise, it is not a good method to make the posteriori error zero. This will force the blind equalizer to compensate for the influence of the noise and then result in a larger misadjustment. Given that noise is inevitable in practice, and inspired by [19], $\nabla_{\boldsymbol{w}^*}\|\boldsymbol{w}(n+1)\|_0$ is used to replace its projection onto the null space of $\boldsymbol{X}^H(n)$. By adopting this process, the updating of the tap coefficient is more flexible, and the algorithm complexity is greatly reduced. Therefore, an updating formula for QAPA-based blind equalization is

$$\boldsymbol{w}(n+1) = \boldsymbol{w}(n) + \mu\boldsymbol{X}(n) \cdot \boldsymbol{A}(n)\boldsymbol{e}^*(n) - \boldsymbol{\kappa}\nabla_{\boldsymbol{w}^*}\|\boldsymbol{w}(n+1)\|_0 \quad (17)$$

The value of $\|\boldsymbol{w}(n+1)\|_0$ is unknown at the n-th iteration. Thus, the approximation is taken to minimize $\|\boldsymbol{w}(n+1) - \boldsymbol{w}(n)\|^2$ so that $\nabla_{\boldsymbol{w}^*}\|\boldsymbol{w}(n+1)\|_0 \approx \nabla_{\boldsymbol{w}^*}\|\boldsymbol{w}(n)\|_0$. However, it is an NP-hard problem to take the derivative of $\|\boldsymbol{w}(n)\|_0$ directly, which is usually approximated by continuous differentiable functions. In this paper, the Laplace function [19] is used for the approximation, and its expression is as follows:

$$\xi(n) = \sum_{i=0}^{qN-1}\xi_i(n) = \sum_{i=0}^{qN-1}\left(1 - e^{-\beta|w_i(n)|}\right) \quad (18)$$

According to the expansion of the first-order Taylor series, the derivative of (18) can be approximated to

$$\frac{\partial\xi(n)}{\partial w_i^*(n)} = \begin{cases} \beta(1-\beta|w_i(n)|)\,\mathrm{sgn}\left[w_i^*(n)\right], & |w_i(n)| \le \dfrac{1}{\beta} \\ 0, & elsewhere \end{cases} \quad (19)$$

By setting $v_i(n) = \partial\xi(n)/\partial w_i^*(n)$, we have $\nabla_{\boldsymbol{w}^*}\|\boldsymbol{w}(n)\|_0 \approx \boldsymbol{v}(n) = \left[v_0(n), v_1(n), \cdots, v_{qN-1}(n)\right]^T$. Then, (17) can be rewritten as

$$\boldsymbol{w}(n+1) = \boldsymbol{w}(n) + \mu\boldsymbol{X}(n) \cdot \left[\boldsymbol{X}^{\mathrm{H}}(n)\boldsymbol{X}(n) + \delta\boldsymbol{I}_L\right]^{-1}\boldsymbol{e}^*(n) - \boldsymbol{\kappa}\boldsymbol{v}(n) \quad (20)$$

where $-\boldsymbol{\kappa}\boldsymbol{v}(n)$ denotes the zero attractor, and it has the advantage of shrinking to zero for the tap coefficients close to zero, without significant reduction for the other coefficients. β is the zero attraction intensity factor.

To further improve the convergence speed of the blind equalizer, the "proportionate" thought is introduced. Considering the MIPAPA in [20], the matrix is introduced as follows:

$$\boldsymbol{P}(n) = \left[\boldsymbol{g}(n-1) \odot \bar{\boldsymbol{x}}(n) \quad \boldsymbol{P}'(n-1)\right] \quad (21)$$

where the operator $\odot$ represents the Hadamard product; $\boldsymbol{P}'(n-1) = [\boldsymbol{g}(n-2) \odot \bar{\boldsymbol{x}}(n-1)\cdots\boldsymbol{g}(n-2) \odot \bar{\boldsymbol{x}}(n-L+1)]$ consists of first $L-1$ columns of $\boldsymbol{P}(n-1)$; $\boldsymbol{g}(n-1) = \left[g_0(n-1), g_1(n-1), \cdots, g_{qN-1}(n-1)\right]^T$ denotes the proportionate coefficient vector, and it can better measure the sparsity of the impulse response in the UWA channel. By assigning different step sizes that are proportionate to the amplitude of tap coefficients, the convergence speed of the equalizer is improved. In addition, we have $g_j(n-1) = \frac{1-\eta}{2qN} + (1+\eta)\frac{|w_j(n-1)|}{2\|w(n-1)\|_1+\varepsilon}$, where ε is a small positive number; $\eta \in [-1, 1)$ represents the regulatory factor, and its ideal values are 0 and -0.5. Obviously, $\boldsymbol{P}(n)$ takes into account the proportionate coefficients of the equalizer at the first $L-1$ instant. Also, it achieves faster convergence speed and less misadjustment than IPAPA [20]. Unfortunately, $\boldsymbol{P}(n)$ cannot directly work on the zero attractor. By adopting degradation processing, the step size is normalized according to the vector of the received signal at the current moment. Finally, the update formula of the blind equalizer of the proposed algorithm (l_0-FS-MIPQAPA) can be expressed as

$$\boldsymbol{w}(n+1) = \boldsymbol{w}(n) + \mu\boldsymbol{P}(n) \cdot \left[\boldsymbol{X}^{\mathrm{H}}(n)\boldsymbol{P}(n) + \delta\boldsymbol{I}_L\right]^{-1}\boldsymbol{e}^*(n) - \boldsymbol{\rho}\boldsymbol{v}(n) \quad (22)$$

where $\rho = \boldsymbol{\kappa}/\left[\bar{\boldsymbol{x}}^H(n)\bar{\boldsymbol{x}}(n) + \delta\right]$.

As can be seen from (22), based on MIPAPA and the structure of FSE, the proposed algorithm allocates different step sizes to all tap coefficients according to their amplitudes. This is conducive to improving the convergence speed of the blind equalizer. By applying the l_0 norm, the tap coefficients close to zero can be adjusted to approach zero faster so that the overall convergence performance of the blind equalizer is improved.

D. CARRIER SYNCHRONIZATION IN NON-FADING CHANNEL

After the fractionally spaced blind equalizer compensates for the UWA sparse multipath channel, the multipath effect is well suppressed. Then, ISI in the output signal $s_r(n)$ is greatly reduced. In this case, it can be considered that the signal is only affected by Gaussian noise. $s_r(n)$ can be expressed as:

$$s_r(n) = Ab_n e^{j2\pi\Delta fnT}e^{j\theta} + z_r(n) \quad (23)$$

where Δf and $z_r(n)$ denote carrier frequency offset and Gaussian white noise, respectively. After the M-power transformation of $s_r(n)$, the demodulated signal is $s_r^M(n)$. $s_r^M(n)$ is a single-frequency signal with Gaussian noise. Its amplitude spectrum has an obvious peak at the frequency of $M\Delta f$, and the phase of the corresponding position indicates the phase offset. Thereby, the values of modulation order, carrier frequency, and phase offset can be estimated. If $S_r(k) = \mathrm{FFT}\left[s_r^M(n)\right]$ and $k_f = \arg\max_k\left[|S_r(k)|\right]$, the estimated values

of the frequency offset and phase offset can be expressed as

$$\begin{aligned} \Delta\hat{f} &= k_f / (M \cdot N_{\mathrm{FFT}}) \\ \hat{\theta} &= \arg\left[S_r\left(k_f\right)\right] / M \end{aligned} \tag{24}$$

where N_{FFT} is the number of sampling points of FFT. The estimation accuracy of the algorithm is limited, so the compensated signal still has a small frequency and phase offset. DPLL is widely used in various systems because of its simple structure and the capacity to track the tiny frequency and phase offset. After the rough compensation through the estimated values above, the second-order decision feedback DPLL [21] that can converge quickly is used to track the carrier phase. After the residual frequency and phase offset are removed, the constellation of the transmitted signal can be obtained. A hard decision is made according to the corresponding mapping rules, and then the information bitstream is recovered. Since the DPLL technology is not the focus of this paper, it will not be discussed in detail here.

IV. SIMULATION RESULTS AND DISCUSSION

In the simulation, the channel h_A is a typical sparse UWA multipath channel given in [22]. Its z-transfer function is $H_A(z) = 1 - 0.5z^{-14} + 0.4z^{-18}$, and its zero plot and amplitude-frequency response are respectively shown in Fig. 3(a) and (b). The zeros of this channel are all located on or near the unit circle. The amplitude-frequency response presents deep fading characteristics, with the maximum fading point up to -18 dB. The channel h_B is generated by the widely used Bellhop channel simulation software based on the popular Argo ocean database. Its z-transfer function is $H_B(z) = 1 + 0.4312z^{-71} + 0.2058z^{-110}$, and its zero plot and amplitude-frequency response are respectively shown in Fig. 3(c) and (d). The coordinates of the selected water region are (165.5°E, 45.5°N). The sound velocity profile and sound ray diagram of this water region are shown in Fig. 4. The sampling rate is set to 8 kHz, and the central frequency is 2 kHz. The transmitter depth, the transmission distance and the receiver depth are 200 m, 5 km and 290 m, respectively. It can be seen that both channels h_A and h_B are obviously sparse, and there are 18 symbols between the first and third path of h_A. The channel h_B is sparser and its coherent bandwidth is smaller than h_A. The maximum propagation delay of h_B is 13.8 ms, and the maximum fading point is -9 dB.

A. BLIND EQUALIZATION PERFORMANCE COMPARISON

To evaluate the effectiveness and anti-noise performance of the blind equalization algorithm proposed in this paper, the channel h_A is selected to transmit the QPSK signal. The proposed l_0-FS-MIPQAPA is compared with the algorithms of VOWL-MMA [3], VS-LMS [4], the FSE-based l_0-FS-IPNLMS [5], and FS-APA [8] by taking the residual ISI as the evaluation criteria. Also, the proposed algorithm is compared with l_0-MMBDFE algorithm [2] based on decision feedback in terms of mean square error (MSE). The order of the equalizer is set to 102. The central tap of the equalizer is

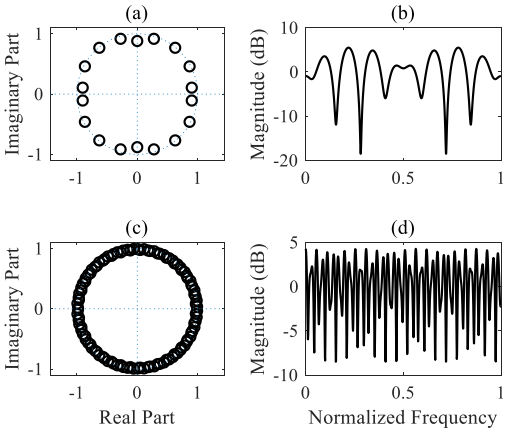

FIGURE 3. The characteristics of the sparse UWA channel: (a) Zero plot of h_A; (b) Amplitude-frequency response of h_A; (c) Zero plot of h_B; (d) Amplitude-frequency response of h_B.

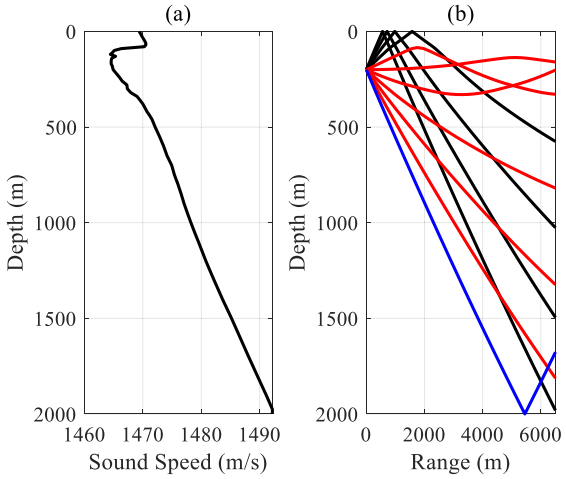

FIGURE 4. The hydrological characteristics of the water region: (a) Sound velocity profile; (b) Sound ray diagram.

initialized to 1 (the two taps in the middle of the $T/2$-spaced equalizer are initialized to 1), and the remaining taps are initialized to 0. As shown in Table 1, the other parameters are set to the values that lead to the optimal performance of the corresponding algorithm. The meaning of characters is consistent with the corresponding reference of each algorithm. Under white Gaussian noise, the residual ISI of the above five algorithms is compared under different SNR values (20 dB and 30 dB). Fig. 5 shows the average residual ISI curves of twenty independent experiments.

It can be seen from Fig. 5 that the performance of the T-spaced VOWL-MMA and VS-LMS algorithms deteriorates seriously in deep-fading sparse UWA multipath channel. When $L = 5$, the convergence speed of the l_0-FS-IPNLMS algorithm is equivalent to that of FS-APA, but both of them outperform the previous two algorithms by exploiting the structure of FSE. The optimal solution of $\boldsymbol{w}(n)$ is the intersection of L hyperplanes composed of column vectors of $\boldsymbol{X}(n)$. APA can make the tap coefficient vector converge to the intersection under the noise-free environment and a large enough equalizer order [8]. Besides, the proposed l_0-FS-MIPQAPA imposes sparse constraints on the taps

TABLE 1. Parameter settings of the six algorithms.

Algorithm	Paper	SNR=20dB	SNR=30dB
VOWL-MMA	[3]	μ=0.1, η_u=0.98, η_u=0.99, q=1, N_0=102	μ=0.15, η_u=0.98, η_u=0.99, q=1, N_0=102
VS-LMS	[4]	α=0.001, β=5, γ=2	α=0.001, β=5, γ=2
l_0-FS-IPNLMS	[5]	μ=0.04, $\gamma=10^{-5}$, η=20, δ=0.01, ε=0.01, κ=0.01	μ=0.05, $\gamma=10^{-4}$, η=10, δ=0.01, ε=0.01, κ=0.01
FS-APA	[8]	μ=0.02, L=5, $\delta=10^{-12}$	μ=0.03, L=5, $\delta=10^{-12}$
l_0-MMBDFE	[2]	μ_f=0.009, μ_b=0.002, N_f=31, N_b=20, α=100, β=0.99	μ_f=0.009, μ_b=0.002, N_f=31, N_b=20, α=100, β=0.99
l_0-FS-MIPQAPA (Proposed algorithm)	/	μ=0.02, L=5, β=5, η=0, $\gamma=10^{-4}$	μ=0.03, L=5, β=10, η=–0.5, $\gamma=10^{-4}$

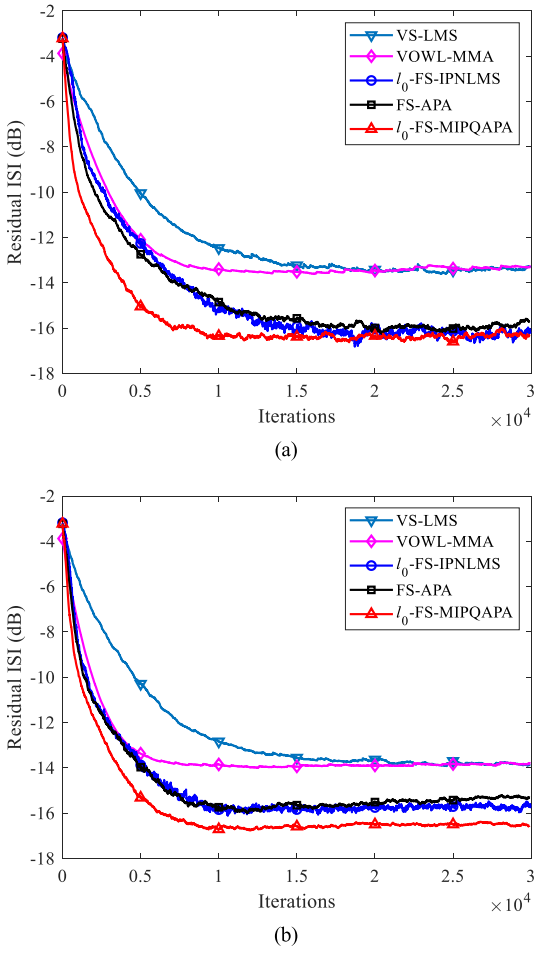

FIGURE 5. Comparison of residual ISI of the five algorithms under channel h_A: (a) 20dB; (b) 30dB.

and assigns different step sizes to all taps according to the amplitude of coefficients. Also, it considers the proportionate history of the previous $L-1$ moments so that the equalizer can approach the intersection at a faster speed in each iteration. At the SNR of 20 dB, the performance of l_0-FS-MIPQAPA is still optimal, indicating that the proposed algorithm is robust to noise. At the SNR of 30 dB, the residual ISI of the proposed algorithm reaches about -16.7 dB, which is the lowest among the five algorithms. Compared with VOWL-MMA and VS-LMS algorithms, the proposed algorithm obtains a performance gain of about 2.5 dB. Besides, the number of iterations required for the convergence of the proposed algorithm is about 4000 times less than that of FS-APA and l_0-FS-IPNLMS.

Fig. 6 shows the MSE performance curves of the proposed algorithm and l_0-MMBDFE algorithm, and the parameters of the two algorithms are listed in Table 1. The MSE results show that the proposed algorithm outperforms the nonlinear l_0-MMBDFE and obtains a performance gain of about 3 dB. The proposed algorithm benefits from the adopted MIPQAPA and FSE. The former makes the tap coefficients reach the optimal solution at a faster speed, while the latter can better compensate the deep-fading UWA channels. Thus, l_0-FS-MIPQAPA converges faster, with a lower steady-state MSE.

To evaluate the performance of the proposed algorithm for different values of projection orders ($L = 3$, 5, and 8), twenty independent experiments are conducted under the SNR of 30 dB, the step size $\mu = 0.03$ and identical equalizer order. The experimental results are shown in Fig. 7. It can be seen that the convergence speed gradually increases with the projection order, but the residual error after convergence increases slightly with the proportionate history. In practice, the computational complexity can be comprehensively considered by selecting the appropriate step size and projection order, to achieve a faster convergence speed and lower residual error.

B. BLIND DEMODULATION PERFORMANCE COMPARISON

To evaluate the validity and practicability of the proposed blind demodulation algorithm under impulsive noise and UWA multipath channel, the proposed algorithm is compared with the blind demodulation algorithms which adopt the blind equalization algorithms in [2], [3] and [4]. Besides, the traditional O&M algorithm is used for timing synchronization in the contrast blind demodulation algorithms. Specifically, the proposed blind demodulation algorithm is compared with the ones in which l_0-MMBDFE [2] (l_0-MMBDFE-Based), VOWL-MMA [3] (VOWL-MMA-Based), and VS-LMS [4] (VS-LMS-Based), are used for blind equalization, respectively. Also, to measure the performance of the proposed blind demodulation algorithm more intuitively, the algorithm is compared under two conditions: 1) the influence of impulsive noise and multipath channel; 2) only the influence of impulsive noise.

Simulation parameters are as follows: the characteristic exponent of α is set to 1.8 and 2.0; the modulation types are

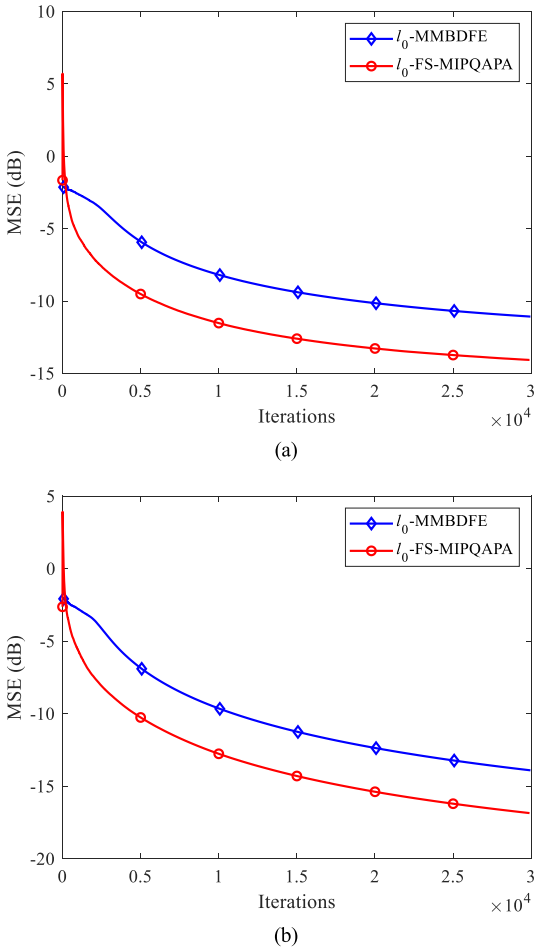

FIGURE 6. Comparison of MSE performance of two algorithms under channel h_A: (a) 20dB; (b) 30dB.

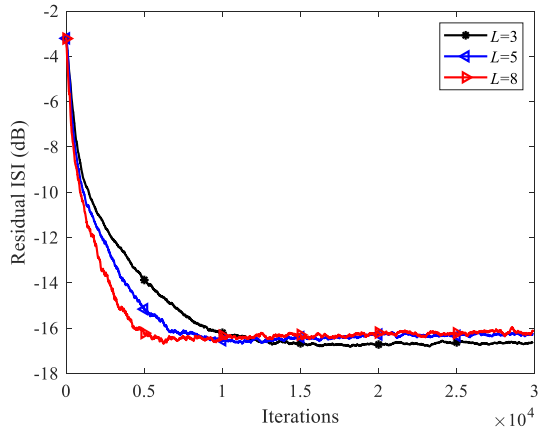

FIGURE 7. Comparison of residual ISI of l_0-FS-MIPQAPA under different projection orders.

QPSK and 8PSK; the channel h_B is selected. The sampling rate, symbol rate, and carrier normalized frequency offset are 8 kHz, 500 Bd and 0.1, respectively. The clock frequency deviation is 2.0×10^{-4}, i.e., 1.6 sampling deviations per second, and the observation time is 2 s and 50 s. For the QPSK signal, the 100 bits in the first 0.1 s are synchronization preamble, and the 1050 bits in the first 0.7 s for the 8PSK

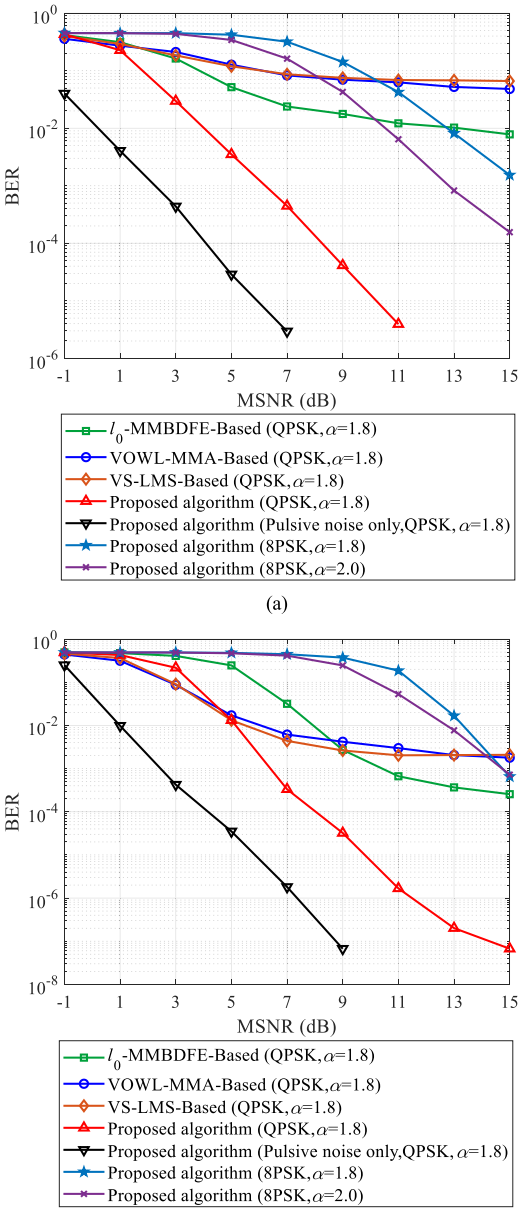

FIGURE 8. Comparison of BER performance of blind demodulation in channel h_B: (a) $t = 2$s (1000 symbols); (b) $t = 50$s (25000 symbols).

signal. The order of the equalizer is set to 82 and initialized with a double spike. The length of each segment signal for the proposed algorithm is $L_0 = 100$. The remaining parameters are set to the values that lead to the optimal performance of the corresponding algorithm. The Monte Carlo simulation test was conducted 300 times under each MSNR, and the average BER curves is shown in Fig. 8.

As shown in Fig. 8(a) and (b), for QPSK signals, if a large clock frequency deviation exists, l_0-MMBDFE-based, VOWL-MMA-based, and VS-LMS-based algorithms cannot track the rapid changes caused by the channel itself and the clock frequency deviation. The reason is that the sampling phase deviation has not been compensated. This significantly reduces the performance of these three algorithms.

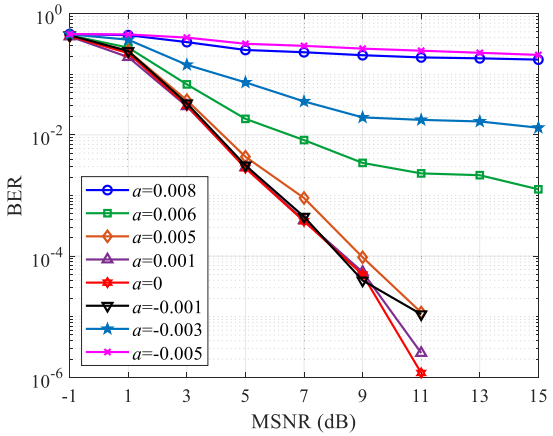

FIGURE 9. Comparison of the BER performance of the proposed algorithm under different Doppler scale factors.

Fig. 8(a) shows the performance comparison with a short observation time of 2 s, compared with VOWL-MMA-based and VS-LMS-based algorithms, the performance of l_0-MMBDFE-based algorithm is improved to some extent by imposing a sparse constraint on the tap coefficients. However, the adopted sparse constraint is not enough to eliminate the influence of large clock frequency deviation and complex UWA channels. Thus, the improvement of demodulation performance is very limited, and there are obvious error floor characteristics.

Besides, when the observation time increases to 50 s, this improvement continues to decrease, as shown in Fig. 8(b). When MSNR $=$ 7 dB, the blind demodulation BER of the proposed algorithm is less than 1.0×10^{-3}, which achieves the MSNR performance gain of 4 dB compared with the l_0-MMBDFE-based one. When MSNR $=$ 13 dB, the performance of the proposed algorithm is about three orders of magnitude better than that of the l_0-MMBDFE-based one. Overall, the blind demodulation performance of the proposed algorithm is superior to other algorithms, and the reasons are summarized as follows.

The proposed blind demodulation algorithm first compensates for the sampling phase deviation caused by clock frequency deviation through more accurate timing synchronization. Then, the signal with two fixed sampling points per symbol is obtained and input to the MIPQAPA-based $T/2$-spaced equalizer with l_0 norm constraint. Finally, the UWA channel can be tracked and compensated quickly, and the original information can be better recovered. It can be seen from Fig. 8 that the performance of the proposed algorithm is similar for the signal observation time of 2s and 50s. It can be concluded that the proposed algorithm is applicable to short burst signals and can avoid taps shift caused by clock frequency deviation or timing error accumulation for a long time. Based on this, the FSE can work continuously without lock-loss.

From the performance comparison results under the above two conditions, it can be seen that the proposed algorithm in the first condition only needs an MSNR gain of about

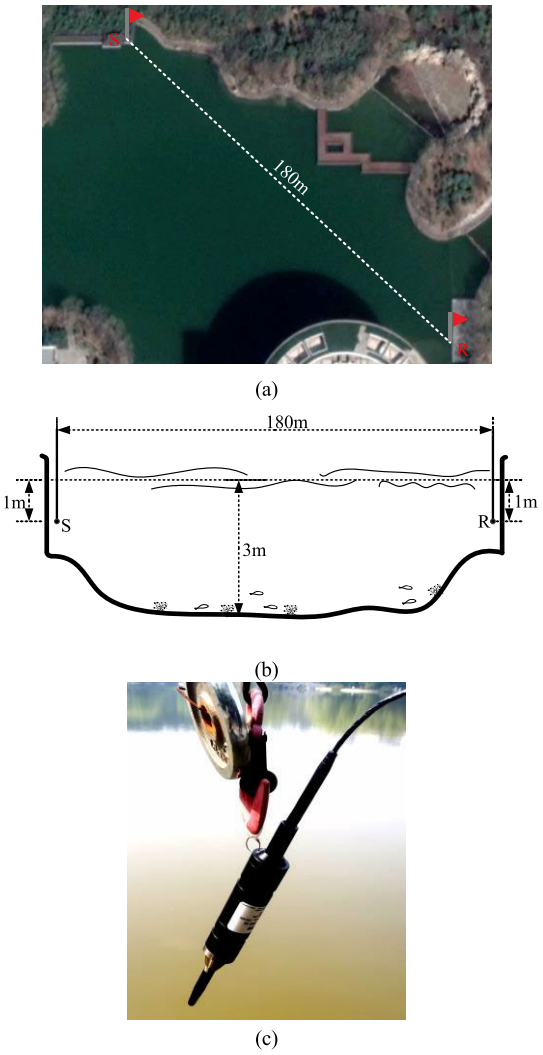

FIGURE 10. The experimental setup of the lake trial: (a) Experiment environment; (b) Location of the experiment equipment; (c) Utilized hydrophone.

4 dB to reach the performance obtained in the second one. However, when the UWA channel is worse than h_B, the performance of the proposed algorithm may degrade, and the MSNR gain required to achieve the same performance will be greater. Compared with the QPSK signal, the Euclidean distance of the 8PSK signal between constellation symbols is smaller, so the hard decision error probability and the BER are higher. In addition, the results show that the proposed algorithm is also suitable for the case of Gaussian noise with the characteristic exponent $\alpha = 2$.

To further evaluate the performance of the proposed blind demodulation algorithm in the time-varying channel, we considered a linear channel with one common Doppler scale. The channel can be modeled as [23]:

$$h(t;\tau) = \sum_{i=1}^{N} A_i \delta(\tau - (\tau_i - at)) \tag{25}$$

The proposed blind demodulation algorithm is tested under different Doppler scale factor a. The signal observation time

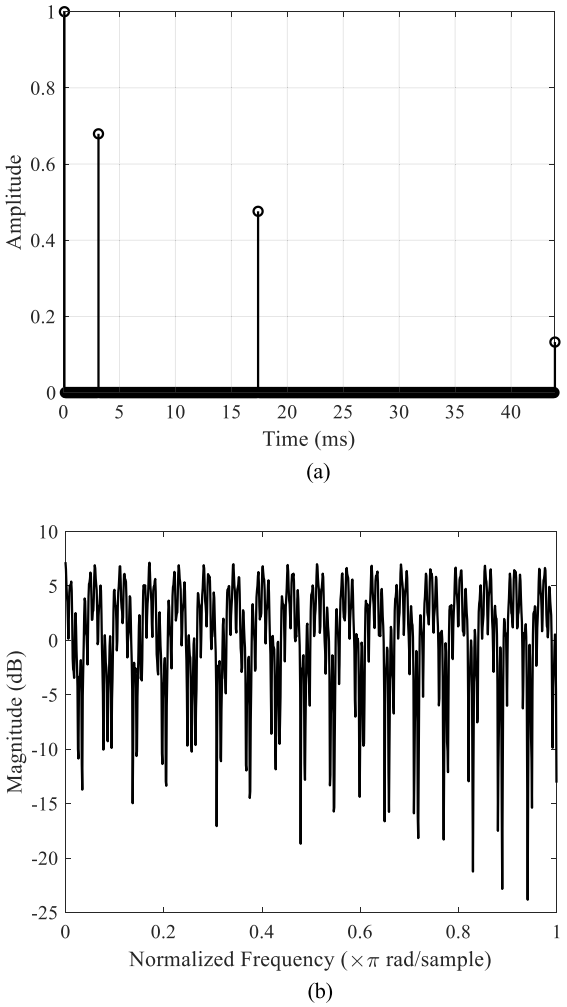

FIGURE 11. The characteristics of the experiment channel: (a) Impulse response; (b) Amplitude-frequency response.

is set to 2s, and the average BER curves are shown in Fig. 9. It can be seen that the algorithm has a good BER performance when the Doppler scale factor is in the range of $(-0.001, 0.005)$. With the gradual increase of $|a|$, the BER performance is getting worse and worse. When $a \geq 0.008$ or $a \leq -0.005$, the algorithm fails, for it cannot compensate for the signal distortion caused by Doppler shift. Overall, the proposed blind demodulation algorithm has some certain robustness in UWA time-varying channel.

The simulation results show that the proposed blind equalization algorithm can effectively compensate for the signal distortion caused by deep-fading sparse UWA multipath channels. Also, the algorithm has a faster convergence speed and lower steady-state error than other algorithms. Besides, the proposed blind demodulation algorithm is more practicable to the UWA MPSK signals under impulsive noise and sparse multipath channel. The clock frequency deviation can be better compensated. In addition, the algorithm is applicable to short burst signals and has a strong capacity for UWA channel tracking and compensation. Moreover, the algorithm is universal for PSK signals with different modulation orders.

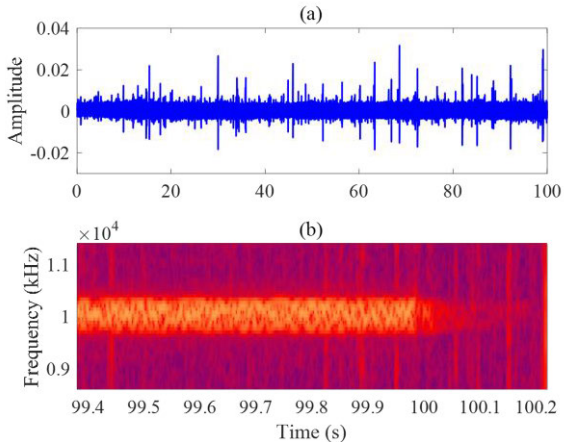

FIGURE 12. The time-domain waveform and time-frequency spectrum of the practical 8PSK signal: (a) Time-domain waveform; (b) Time-frequency spectrum.

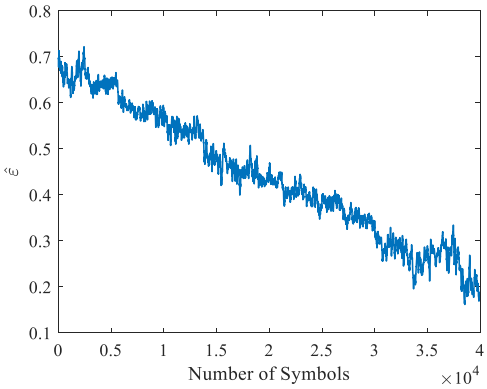

FIGURE 13. The variation curve of timing phase estimation with the number of symbols.

V. PRACTICAL TRIAL AND DISCUSSION

To prove the feasibility of the proposed algorithm in the practical marine environment, a non-cooperative communication trial was conducted in a lake on campus on June 28, 2021 (cloudy to sunny, 31°C∼36°C, breeze). The lake is located in Zhengzhou (113.55°E, 34.82°N). Fig. 10(a) and (b) show the experimental setup. The transmitting node S uses an omnidirectional transducer to simulate the communication side. The receiving node R uses the broadband hydrophone RB9-ETH model (Ocean Sonics) to collect the signals, as shown in Fig. 10(c). The sampling rate is set to 128 kHz, and the transmission distance is approximately 180 m. The transducer and hydrophone are all placed 1 m below the water surface. The deepest part of the lake is about 3 m, as shown in Fig. 10(b).

To measure the environment in the experiment, a linear frequency modulation (LFM) signal is used to estimate the actual channel based on fractional Fourier transform through the method in [24], and the impulse response and amplitude-frequency response of the channel are shown in the Fig. 11(a) and (b), respectively. It can be seen that the channel has obvious sparse and deep-fading characteristics due to multipath effect. The maximum propagation delay of the channel is 44 ms and the maximum fading point is −23 dB.

TABLE 2. The parameters and blind demodulation BER of the four algorithms.

Algorithm	Paper	Parameters	BER
l_0-MMBDFE-Based	[2]	μ_f=0.01, μ_b=0.002, μ=0.001, N_f=21, N_b=17, α=100, β=0.99	9.1835×10^{-3}
VOWL-MMA-Based	[3]	μ=0.1, η_u=0.98, η_u=0.999, q=1, N_0=51	2.5159×10^{-3}
VS-LMS-Based	[4]	α=0.001, β=10, γ=2	4.7553×10^{-3}
Proposed algorithm	/	N=122, μ=0.16, L=8, L_0=100, β=15, η—0.5, $\gamma=10^{-3}$	2.8477×10^{-4}

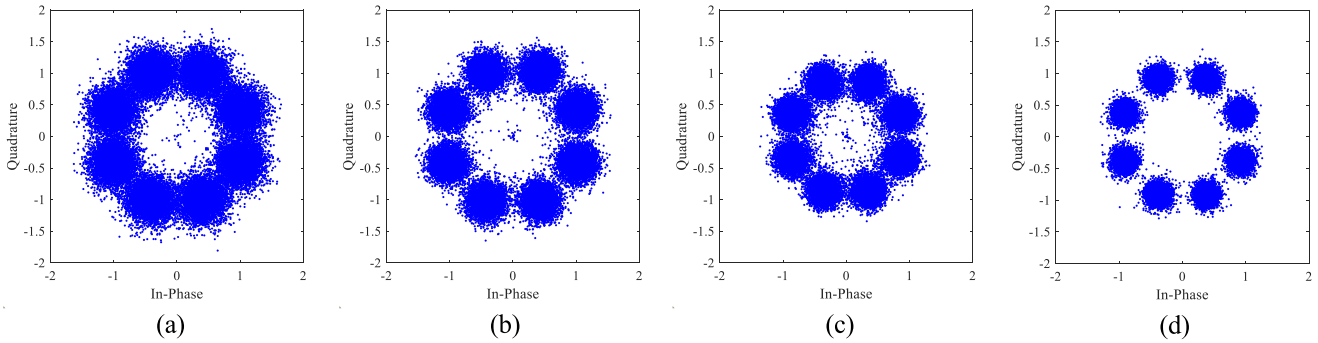

FIGURE 14. The Blind demodulation constellation of the four algorithms: (a) l_0-MMBDFE-Based; (b) VOWL-MMA-Based; (c) VS-LMS-Based; (d) Proposed algorithm.

The 8PSK signal is transmitted under the carrier frequency of 10 kHz and the symbol rate of 400 Bd. The duration of the signal is approximately 100 s, and the number of symbols is about 4.0×10^4. The first 600 bits in the first 0.5 s are synchronization preamble. The time-domain waveform and time-frequency spectrum of the signal is shown in Fig. 12. It can be seen that there is a tail of about 0.2 s at the end of the signal, and there is stronger impulsive noise in the signal. With the method of sample fractiles proposed in [25], the characteristic exponent α is estimated to be about 1.8 for the signal. Using the SDFT-based timing synchronization algorithm, the variation curve of timing phase estimation of each symbol with the number of symbols is obtained and shown in Fig. 13. It can be seen that the change of timing phase estimation from the first symbol to the 3×10^4 symbol is exactly 0.5. Then, it is estimated that the clock frequency deviation of the received signal is about 1.5152×10^{-5}. The clock frequency deviation between sender and receiver is $\Delta F_{\text{clock}} = F_{\text{recv}} - F_{\text{send}} < 0$, where F_{send} and F_{recv} respectively represent the clock frequency of the sender and receiver. Blind demodulation processing is conducted by using the above four algorithms. As shown in Table 2, the parameters are set to the values that lead to the optimal performance of the corresponding algorithm. The constellations of the transmitted signal recovered by each algorithm are shown in Fig. 14. After a hard decision is made on the obtained constellations, compared with the transmitted bitstream, the BER of each algorithm is listed in Table 2.

It can be seen from Fig. 14 that under a small clock frequency deviation, the sampling phase deviation is also small. By comparing Fig. 14(a), (b), (c), and (d), it can be seen that l_0-MMBDFE-based algorithm imposes a sparse constraint on the taps, but its constellation has the worst convergence effect. The reason is that the residual carrier frequency offset in the signal leads to the failure of DFE. VOWL-MMA-based, and VS-LMS-based algorithms have similar performance, but their convergence aggregation effect is still poor. This is because both algorithms are based on the T-spaced, and cannot compensate the deep-fading UWA channel sufficiently. Besides, they do not take into account the sparsity of the channels. Among the four algorithms, the proposed blind demodulation algorithm performs better than the other three algorithms in terms of convergence speed and steady-state error performance. The reasons can be summarized as follows.

The proposed blind demodulation algorithm first compensates for the sampling phase deviation by an SDFT-based accurate timing synchronization. Then, the channel is quickly tracked and compensated by the MIPQAPA-based FSE with sparse constraint. Finally, the M-power transform and DPLL are used to accomplish the carrier synchronization, and the constellation of the original signal is better recovered. It can be seen from Table 2 that the BER of the proposed algorithm is the lowest among the four algorithms, and it is lower an order of magnitude than other algorithms. Meanwhile, the BER of the proposed algorithm is 2.8744×10^{-4} when the synchronization preamble is 200 symbols, which shows that the algorithm is also suitable for burst signals. Overall, the proposed algorithm can blind demodulate the collected practical signals well, further indicating the effectiveness and practicability of the algorithm.

VI. CONCLUSION

In this study, a blind demodulation algorithm is proposed for MPSK signals with impulsive noise and sparse UWA multipath channels. The proposed algorithm is robust to the clock frequency deviation and can effectively compensate for the signal distortion caused by sparse UWA multipath channels. Besides, it can efficiently realize the blind demodulation of

MPSK signals in the marine environment. Compared with the existing algorithms, the proposed algorithm has a higher BER performance, and it is applicable to engineering practice. Theoretical analysis and trial results show that the proposed algorithm is robust and feasible under impulsive noise and UWA channels.

REFERENCES

[1] A. C. Singer, J. K. Nelson, and S. S. Kozat, "Signal processing for underwater acoustic communications," *IEEE Commun. Mag.*, vol. 47, no. 1, pp. 90–96, Jan. 2009.
[2] Z. Liu, L. Jiang, L. Wang, and M. Ke, "An l_0-norm blind decision feedback equalization with adaptive zero attractor for sparse underwater acoustic channel," in *Proc. Int. Wireless Commun. Mobile Comput. (IWCMC)*, Jun. 2021, pp. 1977–1981.
[3] Z. Liu, F. Bai, and Z. Tan, "Variable observation window length blind equalization detector for underwater acoustic communication," *EURASIP J. Wireless Commun. Netw.*, vol. 2020, no. 1, pp. 1–12, Jul. 2020.
[4] J. Sun, X. Li, K. Chen, W. Cui, and M. Chu, "A novel CMA+DD_LMS blind equalization algorithm for underwater acoustic communication," *Comput. J.*, vol. 63, no. 6, pp. 974–981, Jun. 2020.
[5] S. Ma, B. Wang, H. Peng, and T. Zhang, "A variable step size constant modulus algorithm based on l_0-norm for sparse channel equalization," in *Proc. IEEE Int. Conf. Digit. Signal Process. (DSP)*, Oct. 2016, pp. 149–153.
[6] L. Zeng, H. Xu, and T. Wang, "A set-membership like-affine-projection blind equalization algorithm based on data reuse," *Telecommun. Eng.*, vol. 57, no. 2, pp. 230–235, Feb. 2017.
[7] Y.-Z. Jiang and S.-X. Zhang, "Blind adaptive channel equalization based on affine projection algorithm," in *Proc. Int. Symp. Microw., Antenna, Propag. EMC Technol. Wireless Commun.*, Aug. 2007, pp. 1076–1079.
[8] P. S. Diniz, "Blind adaptive filtering," in *Adaptive Filtering: Algorithms and Practical Implementation*, 5nd ed. New York, NY, USA: Springer, 2020, pp. 417–419.
[9] G. Samorodnitsky and M. S. Taqqu, "Stable non-Gaussian random processes: Stochastic models with infinite variance," *J. Amer. Stat. Assoc.*, vol. 90, no. 430, pp. 805–806, Jun. 1995.
[10] Z. Chuangzhan and J. Xin, "Modulation recognition method of communication signals based on correlation characteristics," in *Proc. IEEE Int. Conf. Signal Process., Commun. Comput. (ICSPCC)*, Sep. 2015, pp. 1–5.
[11] A. Zhang, T. Qiu, and X. Zhang, "A new underwater acoustic signals processing approach to a-stable distribution," *J. Electron. Inf. Technol.*, vol. 27, no. 8, pp. 1201–1204, Aug. 2005.
[12] R. Barazideh, W. Sun, B. Natarajan, A. V. Nikitin, and Z. Wang, "Impulsive noise mitigation in underwater acoustic communication systems: Experimental studies," in *Proc. IEEE 9th Annu. Comput. Commun. Workshop Conf. (CCWC)*, Jan. 2019, pp. 880–885.
[13] L. Hui, B.-Q. Dai, and L. Wei, "A pitch detection algorithm based on AMDF and ACF," in *Proc. IEEE Int. Conf. Acoust. Speed Signal Process.*, May 2006, p. 1.
[14] D. J. Artman, S. Chari, and R. P. Gooch, "Joint equalization and timing recovery in a fractionally-spaced equalizer," in *Proc. 26th Asilomar Conf. Signals, Syst. Comput.*, 1992, pp. 25–29.
[15] M. Oerder and H. Meyr, "Digital filter and square timing recovery," *IEEE Trans. Commun.*, vol. 36, no. 5, pp. 605–612, May 1988.
[16] H. Meyr, M. Moeneclaey, and S. A. Fechtel, "Timing adjustment by interpolation," in *Digital Communication Receivers* (Synchronization, Channel Estimation and Signal Processing), vol. 2. New York, NY, USA: Wiley, 2001, pp. 529–530.
[17] C. W. Farrow, "A continuously variable digital delay element," in *Proc. IEEE. Int. Symp. Circuits Syst.*, Jun. 1988, pp. 2641–2645.
[18] Z. Q. T. Luo, M. Meng, K. M. Wong, and J.-K. Zhang, "A fractionally spaced blind equalizer based on linear programming," *IEEE Trans. Signal Process.*, vol. 50, no. 7, pp. 1650–1660, Jul. 2002.
[19] M. V. S. Lima, W. A. Martins, and P. S. R. Diniz, "Affine projection algorithms for sparse system identification," in *Proc. IEEE Int. Conf. Acoust., Speech Signal Process.*, May 2013, pp. 5666–5670.
[20] C. Paleologu, S. Ciochină, and J. Benesty, "An efficient proportionate affine projection algorithm for echo cancellation," *IEEE Signal Process. Lett.*, vol. 17, no. 2, pp. 165–168, Feb. 2010.
[21] Y. Zhang and L. Yu, "Implementation of adaptive blind equalizer with carrier recovery for QAM receiver chip," in *Proc. 6th Int. Conf. (ASIC)*, vol. 1, 2005, pp. 147–152.
[22] L. Zhong and N. Xiao-Ling, "Comparison of equalization algorithms for underwater acoustic channels," in *Proc. 2nd Int. Conf. Comput. Sci. Netw. Technol.*, Dec. 2012, pp. 2059–2063.
[23] S. Zhou and Z. Wang, *OFDM for Underwater Acoustic Communications*, 1nd ed. Chichester, U.K.: Wiley, 2014, p. 13.
[24] J. Yin, J. Hui, P. Cai, and Y. Wang, "Underwater acoustic channel parameter estimation based on fractional Fourier transforms," *Syst. Eng. Electron.*, vol. 29, no. 10, pp. 1624–1627, Oct. 2007.
[25] J. H. McCulloch, "Simple consistent estimators of stable distribution parameters," *Commun. Statist. Simul.*, vol. 15, no. 4, pp. 1109–1136, Jan. 1986.

LULU WU was born in 1993. He received the B.S. degree from the Information Engineering University, in 2014, where he is currently pursuing the master's degree. His research interest includes communication signal analysis and processing.

BIN WANG received the Ph.D. degree from the Information Engineering University, in 2007. She is currently an Associate Professor with the School. Her research interests include underwater acoustic communication signal processing and blind channel equalization.

YAN HUANG received the M.S. degree from the Information Engineering University, in 2007. He is currently a Professor with the School. His research interest includes communication signal analysis and processing.

HAIWANG WANG received the B.S. degree from the Information Engineering University, in 2019, where he is currently pursuing the master's degree. His research interest includes underwater acoustic communication signal analysis and processing.

QIANG TANG received the B.S. degree from the Information Engineering University, in 2019, where he is currently pursuing the master's degree. His research interest includes underwater acoustic localization.